Sensors and Actuators B 203 (2014) 670–676

Contents lists available at ScienceDirect

Sensors and Actuators B: Chemical

journal homepage: www.elsevier.com/locate/snb

Development of nanosized lanthanum strontium aluminum manganite as electrodes for potentiometric oxygen sensor

Max R. Mullen [a], John V. Spirig [a], Julia Hoy [a], Jules L. Routbort [b], Dileep Singh [b], Prabir K. Dutta [a,*]

[a] Department of Chemistry, The Ohio State University, 100 West 18th Avenue, Columbus, OH 43210, United States
[b] Argonne National Laboratory, 9700 South Cass Avenue, Argonne, IL 60439, United States

ARTICLE INFO

Article history:
Received 13 May 2014
Received in revised form 4 July 2014
Accepted 8 July 2014
Available online 18 July 2014

Keywords:
Electrochemical sensor
Oxygen
Potentiometric
YSZ
LSM
High temperature

ABSTRACT

Nanocrystalline $La_{0.8}Sr_{0.2}Al_{0.9}Mn_{0.1}O_3$ (LSAM) was synthesized by a microwave-assisted citrate method, and characterized by electron microscopy and X-ray diffraction. Electrical behavior of LSAM was investigated by impedance spectroscopy and activation energy of conduction was obtained. Joining of sintered bodies of LSAM and yttria-stabilized tetragonal zirconia polycrystals (YTZP), an extensively studied oxygen ion conducting electrolyte, was examined by isostatic hot pressing methods. Characteristics of the joining region were evaluated with microprobe Raman spectroscopy, and products formed at the interface, primarily strontium zirconate, was confirmed by examination of high temperature chemical reaction between LSAM and YTZP powders. The electrical properties of the LSAM were exploited for development of a high temperature oxygen sensor in which LSAM functioned as the electrode and YTZP as electrolyte.

1. Introduction

Yttria-stabilized zirconia (YSZ), because of its oxygen-ion conducting property is used as an electrolyte for oxygen sensors and solid oxide fuel cell (SOFC) applications. Platinum is typically used as an electrode material for oxygen sensors. However, for SOFC, there are a variety of electrodes that are being studied. Amongst these, lanthanum strontium manganite $La_{1-x}Sr_xMnO_3$ (LSM, $x = 0.1$–0.3 most commonly), an ABO_3 perovskite, is frequently used as a cathode because of its oxygen reduction characteristics and high electronic conductivity at fuel cell operating temperatures (600–1000 °C) [1,2]. The triple point boundaries (TPB) between YSZ, LSM and oxygen are active sites for oxygen reduction, much like Pt, YSZ, and oxygen TPB for oxygen sensors. A significant hurdle with the use of LSM is its reaction with YSZ to form insulating pyrochlores lanthanum zirconate ($La_2Zr_2O_7$) and strontium zirconate ($SrZrO_3$). In order to reduce formation of an insulating interlayer between LSM and YSZ [3–7], previous studies have doped out varying amounts of the B site Mn in LSM for Al, $La_xSr_{1-x}Al_yMn_{1-y}O_{3-\delta}$ [6–8].

Another potential use of electroceramic materials is in the area of oxygen sensors [9]. We have reported earlier on use of lanthanum strontium iron cobalt oxide as an electrode for an oxygen sensor [10]. Use of composite lanthanum strontium manganite and YSZ as an oxygen sensor electrode resulted in internally reference sensors stable over a period of 6600 h [11]. Other internally referenced sensors have also been fabricated, by Kaneko [12], van Setten [13] and Zhuiykov [14]. We have also reported on an oxygen sensor, in which the reference cavity was formed by joining of two YSZ pieces by grain boundary sliding [15]. In all of these designs, some sort of a glass frit is used to seal the cavity, e.g. in our design the internal reference electrode (typically Pt) breached the YSZ joints, and this cavity was sealed with a glass seal. Such glass seals soften at around 800 °C, and limit the use of such devices to temperatures below this limit. An electroceramic material that can act as an internal reference electrode and at the same time form a hermetic seal with an electrolyte like YSZ will make possible design of air-reference free oxygen sensors that can operate at temperatures >800 °C.

In this study, we focus on synthesis of nanometer-sized aluminum-doped $La_{0.8}Sr_{0.2}Al_{0.9}Mn_{0.1}O_3$ (LSAM) using a microwave-assisted hydrothermal method. Prado-Gonjal [16] used this method to produce nanoparticles of several lanthanum based perovskites, including $LaAlO_3$, $LaMnO_3$, and $La_{0.8}Sr_{0.2}FeO_3$. Lanthanum manganites incorporating Sr and Gd were also synthesized by microwave methods [17,18]. These methods are very

Abbreviations: LSAM, $La_{0.8}Sr_{0.2}Al_{0.9}Mn_{0.1}O_3$.

* Corresponding author. Tel.: +1 614 292 4532.
E-mail addresses: dutta@chemistry.ohio-state.edu, dutta.1@osu.edu (P.K. Dutta).

http://dx.doi.org/10.1016/j.snb.2014.07.027
0925-4005/

similar to the Pechini synthesis, also used to make lanthanum based perovskite nanoparticles for sensing applications [19], however the hydrothermal step occurs in a microwave. We examine the electrical and mechanical properties of nanoparticulate LSAM. The nanosize of LSAM should influence its joining with other electroceramics and is examined. There have been two previous studies on high pressure joining of micron-sized LSAM to yttria stabilized tetragonal zirconia polycrystals (YTZP), a form of YSZ. Spirig et al. reported that the joint was produced by grain boundary sliding, and found no spectroscopic evidence for any product at the joint surface. Pappacena et al. examined a different LSAM composition ($La_{0.8}Sr_{0.2}Al_{0.5}Mn_{0.5}O_3$), but still micron-sized, and reported a strong joint with YTZP, but noted that an intermediate Sr containing layer was cementing the joint. We follow the high pressure and temperature bonding between nanoparticulate LSAM and YTZP by microprobe Raman spectroscopy. LSAM was bonded to YTZP by isostatic hot pressing methods and its properties as an electrode for an oxygen sensor is examined, a concept previously proposed but not yet reduced to practice [6,7].

2. Materials and methods

2.1. Synthesis, physical, and electrical characterization

$La_{0.8}Sr_{0.2}Al_{0.9}Mn_{0.1}O_3$ was prepared by a microwave-assisted hydrothermal method. Nitrate salts of lanthanum $La(NO_3)_3{\cdot}6H_2O$ (Alfa Aesar), strontium $Sr(NO_3)_2$ (Alfa Aesar), aluminum $Al(NO_3)_3{\cdot}9H_2O$ (Aldrich), and manganese $Mn(NO_3)_2{\cdot}xH_2O$, x = approximately 4 (Alfa Aesar) were combined in the stoichiometric ratio 0.8:0.2:0.9:0.1 respectively. To an aqueous solution of these salts was added citric acid monohydrate (Fischer Scientific) in equimolar ratio to the sum of all metal salts. The pH of the solution was then buffered at pH 9.0–9.1 using ammonium hydroxide (Certified A.C.S. Plus, Fischer Scientific).

The synthesis was carried out in a CEM Mars 5 microwave reactor with HP500 Plus reaction chambers. The microwave was set to 200 °C and then dwelled for 6 h. The slurry was then heated in air (95 °C) then under vacuum (100 °C) to remove excess water. The resultant hard brittle solid was ground in a mortar and pestle, ball milled, and calcined in air at 650 °C for 2 h. The resultant low density solid was then ground in a mortar and pestle to a fine powder and pressed into pellets.

SEM micrographs were obtained on a Philips XL-30 ESEM. Samples were prepared by cutting a cross section, grinding with 240, 320, 480, and 600 grit, and then polishing down to 1 μm polish. The cross section was then thermally etched in air at 1200 °C for 3 h to reveal the grains. TEM micrographs were obtained on a Tecnai F20 transmission electron microscope on a lacy carbon grid. XRD was performed on a Rigaku Geigerflex diffractometer using monochromated Cu Kα (λ = 1.5405 Å) radiation and 2 mm, 1 mm, 3 mm slits.

Impedance experiments were performed on a Solartron 1260 impedance/gain-phase analyzer impedance measurement system inside a Lindburg Blue tube furnace. Experiments were performed between 100 and 300 mV AC under varying temperatures (500–800 °C) in air and nitrogen. The applied frequency was 0.1–10^7 Hz. No DC voltage was applied. Samples were prepared in a pellet press using a bar mold. Samples were sintered at 1500 °C for 50 h.

The Arrhenius equation (1) was used to determine activation energy of a process where A is an exponential factor, T is the temperature, R is the ideal gas constant, and E_a is the activation energy.

$$\ln(\sigma_e T) = A + \frac{-E_a}{RT} \quad (1)$$

2.2. Chemical reactivity of $La_{0.8}Sr_{0.2}Al_{0.9}Mn_{0.1}O_3$ and YSZ

YSZ powder (TOSOH) was thermally treated for 14 h at 1300 °C. Equimolar quantities of YTZP and LSAM powder were combined and ball milled. The resultant powder was formed into a pellet in a 1.3 cm die and pressed under 3000 kg for 20 min. The pellet was sintered at 1300 °C for 3 h in Ar using the same heating profile used during joint fabrication. The pellet was then crushed and ball milled. The final sintered powder was examined by XRD.

2.3. Joining of $La_{0.8}Sr_{0.2}Al_{0.9}Mn_{0.1}O_3$ and YTZP

The YTZP for the joint was made with pellets made from nanoparticles of YTZP 3% from Tosoh (Japan). The LSAM was pellet pressed and then densified for 50 h at 1500 °C in air. Both sides of each pellet were coarse ground to a 600 grit polishing paper. One side of each was then polished down to a 1 μm polish. The two pellets were loaded into an Instron Universal Testing Machine with the mirror polished sides facing and protected above and below by graphite foil. The chamber was evacuated and flushed with argon gas three times and then maintained in an Ar atmosphere. A load of 50 N was applied while the chamber was heated to temperature (1250–1350 °C) to ensure maintained load on the sample. After dwelling at temperature for at least 45 min a steady state strain rate of 1.5–4.5 × 10^{-5} mm/mm was applied to the samples. For sensor fabrication, samples were also joined by a steady state stress method, where stress was ramped linearly (0.5 MPa/h) to a final stress and then relieved.

2.4. Raman spectroscopy

Raman spectroscopy was performed with a Renishaw Raman Microprobe using a 514 nm laser wavelength. Reference spectra were obtained on powders and mapping experiments were performed on a polished cross section of a joined sample. Mapping experiments were performed with a 100× objective over a 30 μm × 6 μm area using 1 μm steps in both the "x" and "y" directions. The long edge of the Raman mapping ran perpendicular to the sample interface.

2.5. Sensor fabrication and sensing experiments

A pellet of LSAM sintered at 1500 °C for 50 h was joined to a pellet of sintered commercial YTZP by the methods described above. Porous platinum electrodes were then attached with platinum ink and wires to the center of the top and bottom of the joined samples. The joined sample was then mounted onto the end of a quartz tube with Ceramabond 552 alumina paste (Aremco). The pores of the alumina paste were filled with Ceramabond 617 glass sealant paint (Aremco). Pt lead wires were run along the inside of the quartz tube to the platinum electrode and a lead wire was connected to the LSAM electrode on the outside of the tube. Oxygen sensing experiments were performed in a Lindburg Blue tube furnace Type TF55035A with an Agilent LXI data acquisition/switch unit and in house LabVIEW software and Sierra mass flow controllers for mixing gases. Sample gas mixtures (1–21% O_2 breathing air mixed with 4.8 N_2) were flowed at 100 sccm outside of the quartz tube in the tube furnace chamber. The interior of the quartz tube was left open to lab air as a reference.

3. Results

3.1. Synthesis of nanoparticulate LSAM

Nitrates of lanthanum, strontium, aluminum, and manganese were dissolved in distilled water with molar ratio of

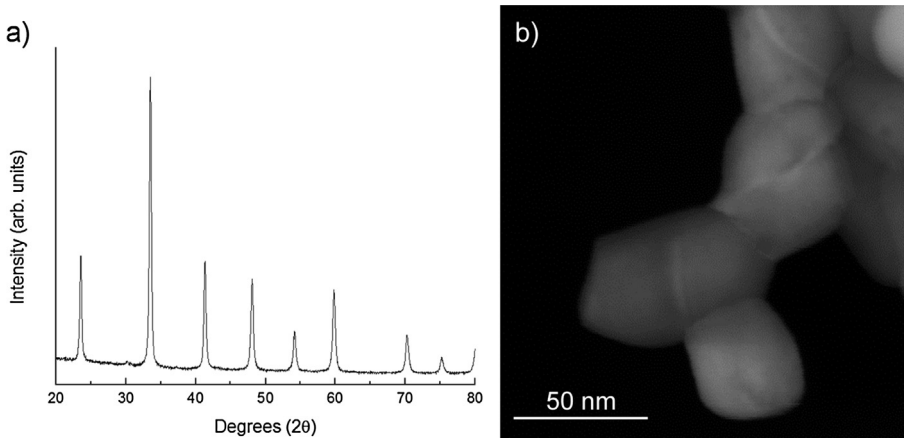

Fig. 1. Physical properties of LSAM nanoparticles: (a) powder diffraction pattern and (b) TEM.

8:2:9:1 respectively, to provide LSAM with a composition of $La_{0.8}Sr_{0.2}Al_{0.9}Mn_{0.1}O_3$. To this solution was added citric acid in a 1:1 charge balance with the metal cations, the role of the citric acid being to complex the ions. Hydrothermal treatment of reagents (200 °C) in the microwave was carried out to initiate the reaction. The material was then dried to a brown solid. Calcination at 650 °C for 2 h ignited the material and the result was a fine green powder. Further sintering at 1500 °C resulted in a dark gray material.

3.2. Physical characterization of nanoparticulate LSAM

Fig. 1a shows an X-ray diffraction pattern of the LSAM product. The location and relative height of the peaks (23.4°, 33.3°, 41.1°, 47.9°, 54.0°, 59.6°, 70.0°, 75.0°, 80.0°, 2θ) are consistent with a cubic perovskite crystal structure (Pm−3m) with a lattice constant of 3.84 Å [6]. The size of the LSAM particles was also determined by transmission electron microscopy (TEM) to be approximately 40 nm (Fig. 1b).

Impedance spectroscopy over the frequency range of 0.1–10^7 Hz was carried out with sintered pellets of LSAM in both air and N_2 over the temperature range of 500–800 °C. Fig. 2a shows the Nyquist plots obtained in air. The plots exhibit a slight depression, but only a single semicircle could be discerned. The intercept on the Z' axis was considered to be the total impedance, and conductivity was derived from this intercept. Table 1 compares the total conductivity for air and N_2 (impedance data and Arrhenius plot for N_2 is shown in supplementary section, Fig. 1S). Based on these conductivity data at various temperatures, an activation energy (E_a, Fig. 2b) was derived and listed in Table 1. The increasing conductivity with temperature is indicative of semiconducting behavior. The change in conductivity from air to N_2 was a decrease by a factor of two, demonstrating a weak dependence of conductivity on pO_2. The activation energies in air and N_2 were also similar (~86 kJ/mol). The density of pellets used in conductivity experiments was determined to be 88.3% of theoretical density.

3.3. Chemical reactivity of nanoparticulate LSAM with YTZP

An equimolar mixture of YTZP and LSAM powders was pelletized and reacted in Ar at 1300 °C for 14 h. Fig. 3 shows the XRD of the product of the reaction.

A lack of reflections at 28.7° and 35.6° 2θ indicate that lanthanum zirconate (JCPDS# 17-0450) or strontium oxide (JCPDS# 65-2652), respectively are not forming. Strontium zirconate formation was however noted by reflections at 30.84°, 44.13°, and 53.98° 2θ (indicated by arrows in Fig. 3). Reaction between lanthanum strontium manganite and yttria stabilized zirconia at 1000 °C in nitrogen is reported to result in strontium zirconate formation [5]. The presence of aluminum in LSAM did not therefore completely inhibit reaction. Another notable change is the disappearance of the monoclinic phase in the YTZP, observable due to a loss of peaks at 28.48° and 31.58° 2θ [20]. This is to be expected because YTZP (~3% yttria) that has been sintered at 1250 °C or above loses its monoclinic phase [21]. For this range of yttria doping, tetragonal is the high temperature stabilized phase.

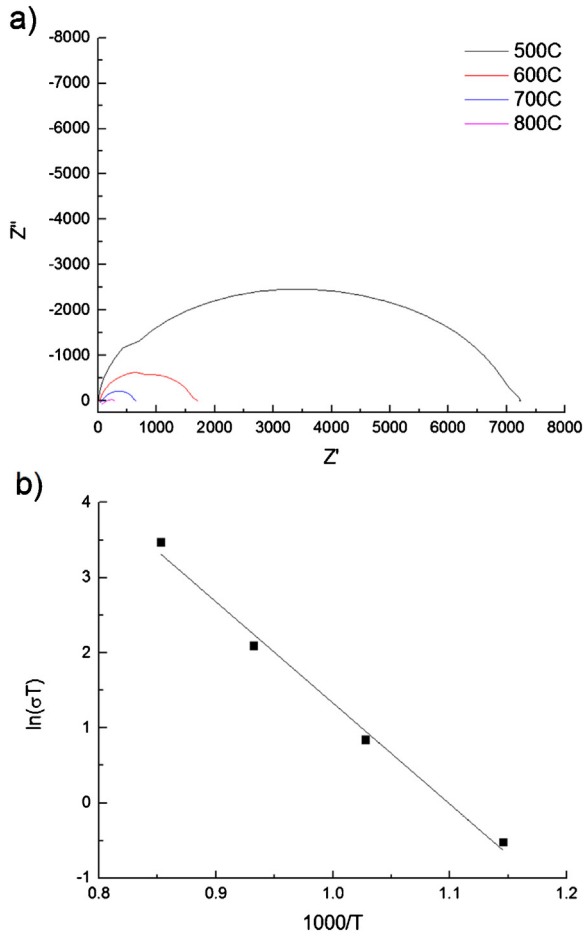

Fig. 2. Electrical characterization of sintered LSAM nanoparticles: (a) Nyquist plots and (b) Arrhenius plot from which activation energy is acquired in air (the impedance value used for determination of activation energy was the resistance of the low frequency intercept minus the resistance of the high frequency intercept).

Table 1
Electrical properties of LSAM in air and nitrogen.

Gaseous environment	Activation energy (kJ/mol)	Conductivity at 500 °C (S cm^{-1})	Conductivity at 600 °C (S cm^{-1})	Conductivity at 700 °C (S cm^{-1})	Conductivity at 800 °C (S cm^{-1})
Air	86.3	1.2E−03	5.1E−03	1.4E−02	3.8E−02
Nitrogen	86.4	5.3E−04	2.3E−03	6.8E−03	1.6E−02

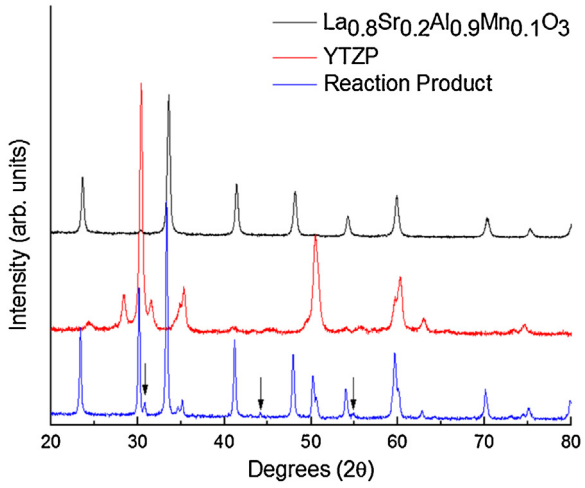

Fig. 3. Powder diffraction patterns of TOSOH YTZP powder, LSAM and a mixture of the two milled together, pelletized, and subjected to 1300 °C (arrows indicate new species $SrZrO_3$).

3.4. Joining of nanoparticulate LSAM with YTZP

Polished pellets prepared from powders of LSAM and YTZP were isostatically pressed at 1350° C with varying strain rates of 1.5–4.5 × 10^{-5} s^{-1}. Fig. 4 shows the stress versus strain curve of an example of one such joining where LSAM and nano-YTZP samples were joined using a 3.0 × 10^{-5} s^{-1} strain rate at 1350 °C. The sloping off of the straight line in the stress strain curve indicates the onset of plastic deformation below 6 MPa. This value is lower than the 10 MPa stress previously reported for joint formation of micron-sized LSAM and YTZP at 1350 °C [6]. The overall change in sample height was 3.8% plastic deformation with similar changes in the height of the LSAM and YTZP layers indicating plastic deformation in both layers.

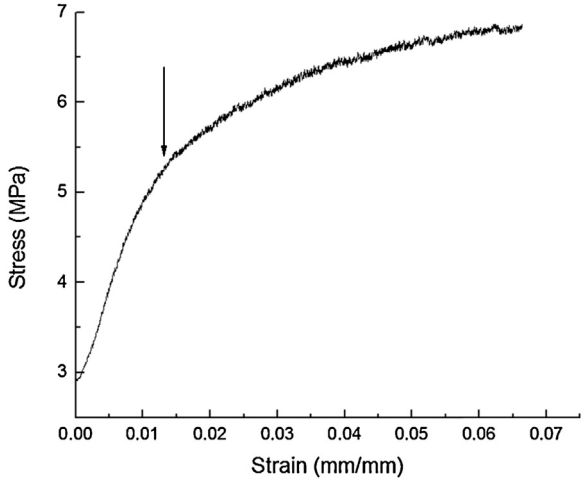

Fig. 4. Stress vs. strain curve for LSAM and nano-YTZP pressed pellets show onset of plastic deformation below 6 MPa (arrow indicates this onset).

Fig. 5 is a cross sectional SEM image of the joined sample and four distinct layers are observed. To the left of the figure are four Raman spectra collected from the four distinct layers. These Raman bands were assigned by comparison with pure compounds (see supplementary section, Figs. 2S–5S). They are assigned as LSAM at the top, strontium zirconate in the upper middle, cubic zirconia in the lower middle, and YTZP on the bottom. It is reported that lanthanum and strontium in LSM will form zirconates by reaction with YSZ, and that manganese diffuses into the grain boundaries between YTZP particles to form larger grains of cubic manganese containing YSZ [5].

3.5. Sensor fabrication and testing

Fig. 6 shows a diagram of the oxygen sensor examined in this study. LSAM was deposited on the electrolyte YTZP from a slurry, and heated to 1350 °C. However, the LSAM did not bind well to the YTZP, and the particles fell off. When a pellet of LSAM was bonded to YTZP at 1250 °C by applying a steady state stress rate of 0.5 MPa/min for 100 min, a stable sensing electrode was formed. The LSAM-YTZP bi-layer was mounted on the end of a quartz tube inside a larger quartz housing, all contained within a heated environment. The outer sensing environment was maintained at different concentrations of O_2. The sensor responded reproducibly to steps from 21% to 10%, 5%, 2%, and 1% O_2 and back in the temperature range of 600–800 °C. Fig. 7a shows a sensor trace at 700 °C and the response at each concentration of O_2 is Nernstian, as shown in Fig. 7b.

4. Discussion

4.1. Synthesis of nanoparticulate LSAM

We report here a microwave-assisted hydrothermal method to synthesize nanometer sized LSAM. Previous methods for LSAM synthesis involved high temperature solid state reaction with intermittent grinding [6–8]. Intermediate grinding required the cooling of the sample, grinding, then reheating to temperature, which added substantial processing time. This method resulted in micron-sized particles with phase inhomogeneity if the intermediate grinding is not accomplished properly. The choice of microwave-assisted hydrothermal synthesis was based on shorter synthesis time (hours) as compared to solid state methods, nanosize product yield (tens of nanometers), and product phase purity [16–18]. This last point is particularly important because La_2O_3, an oxide that forms as a byproduct if reaction is not complete, will react with YSZ to produce lanthanum zirconate ($La_2Zr_2O_7$) [4]. Based on Fig. 1, it is clear that the microwave-assisted hydrothermal citrate method is effective at preparing single phase $La_{0.8}Sr_{0.2}Al_{0.9}Mn_{0.1}O_3$ nanoparticles, with average particle size of about 40 nm.

4.2. Joining of nanoparticulate LSAM with YTZP

Joining of ceramics can occur by diffusional bonding, grain boundary sliding (GBS) super plastic deformation, and reaction bonding. Some ceramics materials that are sufficiently small in particle size can deform plastically or superplastically at low temperature ($T_{max} \sim 0.6\,T_m$ where T_m is the melting point of the ceramic) when a load is applied [22–27]. During deformation two

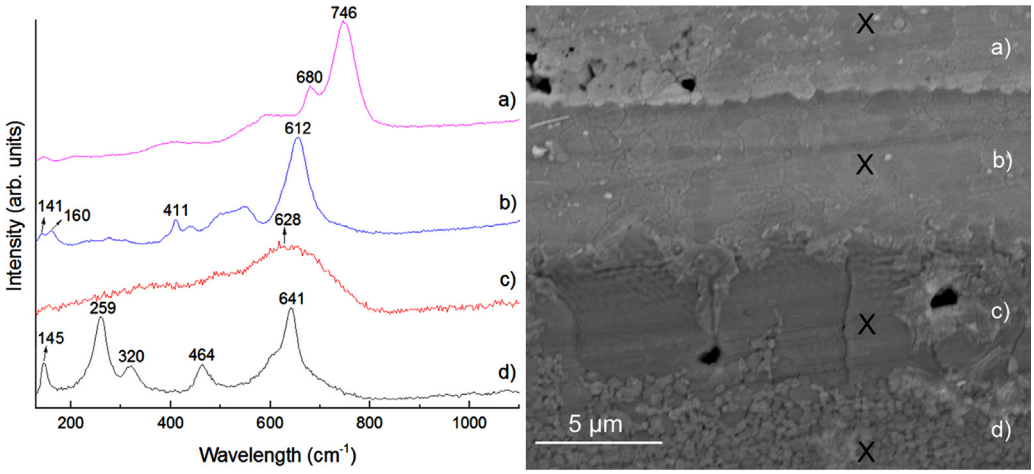

Fig. 5. SEM of joined sample with representative Raman spectra. The layers are marked as (a) top layer, (b) upper middle layer, (c) lower middle layer, and (d) bottom layer. The "X"'s on the SEM image indicate the approximate distance from the interface of (b) and (c) where the spectra were taken.

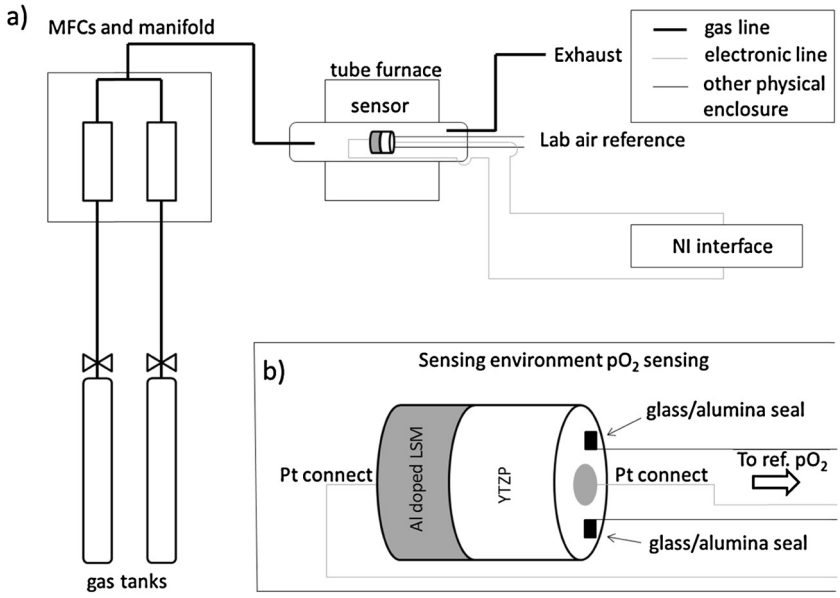

Fig. 6. Diagram of sensor showing gas and electrical lines where (a) focuses the equipment and instrumentation associated with the experiment and (b) focuses on a close up of the sensor itself inside a quartz tube sensing environment mounted in the tube furnace.

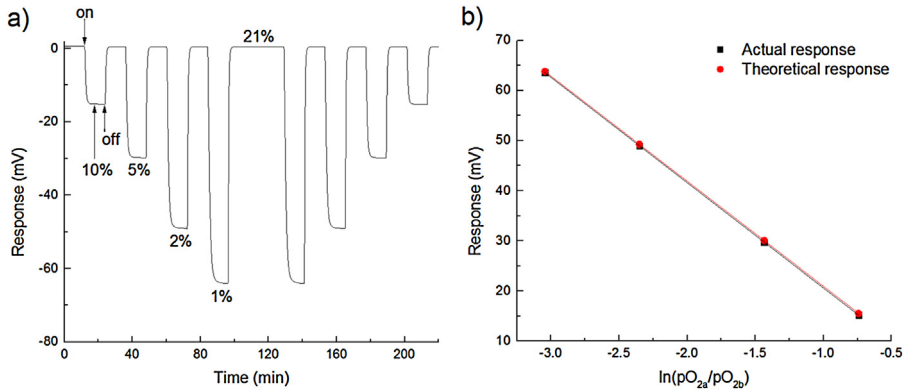

Fig. 7. Potentiometric sensing data for a sensor based on YTZP and LSAM. Sensor (a) trace with a baseline 21% oxygen in a balance of nitrogen flowing against a reference of lab air. The percentage listed next to the perturbation in response voltage is the new concentration of O_2 flowing into the sensing environment. Off indicates a switch back to 21%. Plot (b) shows that the response of the sensor is Nernstian.

discreet bodies can be bonded or "joined" whereby the particles at the interface of each material migrate into one another. The viability of a particle to engage in plastic and superplastic creep mechanisms when joining with another material is inversely related to size of the particle [28], given in Eq. (2):

$$\dot{\varepsilon} = A\frac{Gb}{kT}\left(\frac{b}{d}\right)^{p}\left(\frac{\sigma}{G}\right)^{n} D \quad (2)$$

where $\dot{\varepsilon}$ is the steady state strain rate, or creep rate, G is the shear stress, b is the magnitude of the Burges vector, d is the grain size, k is the Boltzmann constant, T is the temperature, σ is the stress, D is related to the diffusion coefficient, and p and n are the grain size and stress exponents respectively. Since we were able to reduce the grain diameter of LSAM by two orders of magnitude using the microwave method, the joining process should be facilitated as compared to previous studies with micron-sized LSAM particles [6,7]. Fig. 4 shows the onset of plastic deformation of samples containing sintered bodies of LSAM and YTZP, both from nanoparticulate sources at 1350 °C. Plastic deformation was readily observed as a sloping off in the stress vs. strain data and occurred at lower pressures as compared to micron-sized LSAM, due to the decreased grain size. The SEM image in Fig. 5 shows a 5 μm region of strontium zirconate (Fig. 5b) and 5 μm region of cubic YSZ (Fig. 5c) at the joint interface, formed by B site leaching from the LSAM (Fig. 5a) into neighboring YTZP (Fig. 5d). The formation of these intermediates at the joint plane is consistent with the chemical reaction between mixtures of fine-grained YTZP and LSAM at 1300 °C, which also leads to formation of strontium zirconate, as seen in Fig. 3. Previous studies with micron-sized $La_{0.8}Sr_{0.2}Al_{0.5}Mn_{0.5}O_3$ with lower levels of Al have reported the formation of strontium zirconate [7]. Surface segregation of Sr has been noted in LSAM, especially for samples heated to 1250 °C and can possibly exist as SrO [7]. The top most and bottom most layers of LSAM and YTZP in Fig. 5 however do not appear reacted beyond about 5 μm out from the joint plane. The particles in these areas are not substantially deformed from spheres. This shape factor, as well as the low stress required to join the samples, indicate that both the LSAM and YTZP deformed superplastically, however ultimately a reaction based joint is being formed.

4.3. Application of nanoparticulate LSAM as an electrode for oxygen sensor

Our objective was to use the LSAM as an electrode with YTZP as electrolyte for sensing of oxygen. In that context, the nature of conductivity of LSAM is relevant. LSM is well known as an electronic conductor with conductivity of 115–123 S cm^{-1} at 800–950 °C, with ionic conductivity of 5.7×10^{-7} S cm^{-1} at 800 °C (pO_2 = 1 atm) [1]. The high electron conductivity stems from polaron hopping between Mn^{3+}–O–Mn^{4+} chains. Lanthanum strontium aluminate (LSA) is a p-type semiconductor at high partial pressures of oxygen ($pO_2 > 10^{-2}$ atm), and becomes increasingly ionically conductive at low partial pressures of oxygen, with pure ionic conductivity at $pO_2 = 10^{-9}$ atm [29,30]. Thus, under the conditions of the present study (pO_2 = 0.01–0.2 atm), even LSA would primarily function as an electronic conductor. However, with a further 10% Mn doping as in LSAM, the electronic conductivity should increase further. Literature values of conductivity of LSA at 800 °C in air is 3.3×10^{-3} S cm^{-1} [30], as compared to LSAM of 3.8×10^{-2} S cm^{-1} (Table 1), a factor of 10 increase due to the Mn doping. As Table 1 indicates, there is a weak effect of conductivity on pO_2 (factor of two less in N_2 as compared to air) suggesting electronic conductivity and the E_a between air and N_2 are comparable (86 kJ/mol). Also, the increase of conductivity with temperature is indicative of semiconducting behavior. The high content of Al^{3+} in LSAM still leads to a lower conductivity by about 4 orders of magnitude as compared to LSM with a similar composition ($La_{0.85}$–$Sr_{0.15}$) and porosity [31].

The LSAM if deposited on the sintered YTZP pellets as a slurry did not stick to the YTZP surface even after sintering at 1250 °C. However, if the LSAM was bonded on to the YTZP surface by applying pressure (stress method with the rate of change in pressure with time being constant) at 1250–1350 °C, a bond between the LSAM and YTZP could be established. Fig. 7a and b shows the sensing data with a Nernstian response. The Nernstian response of the sensor with LSAM/YTZP electrode/electrolyte interface indicates that

- LSAM (even with the high Al content) has sufficient conductivity to serve as an effective electrode.
- Porosity of LSAM is providing the diffusion of oxygen into the TPB.
- The LSAM-YTZP joint produced by the isostatic press is robust.
- The interfacial reaction between YTZP and LSAM formed upon joining does not compromise sensor signal or response time within the restraints of the time constant of our system.

5. Conclusions

Hydrothermal synthesis of $La_{0.8}Sr_{0.2}Al_{0.9}Mn_{0.1}O_3$ (LSAM) yielded nanosize particles and exhibited reactivity with YTZP. These LSAM particles were found to be electrically conductive in the range of 600–900 °C. LSAM was joined by diffusion and reaction bonds to various types of YTZP at 1250–1350 °C by isostatic hot pressing methods. To demonstrate that LSAM can act as a high temperature electrode material with YTZP electrolytes, a pressure-assisted joined LSAM-YTZP was used successfully in high temperature oxygen sensing experiments in a range of 1–21% O_2.

Acknowledgments

The authors would like to express their gratitude to the National Science Foundation (NSF-PFI 1318136) for support of this research.

Appendix A. Supplementary data

Supplementary data associated with this article can be found, in the online version, at http://dx.doi.org/10.1016/j.snb.2014.07.027.

References

[1] S. Jiang, Development of lanthanum strontium manganite perovskite cathode materials of solid oxide fuel cells: a review, J. Mater. Sci. 43 (2008) 6799–6833.
[2] C.-C.T. Yang, W.-C.J. Wei, A. Roosen, Electrical conductivity and microstructures of $La_{0.65}Sr_{0.3}MnO_3$–8 mol% yttria-stabilized zirconia, Mater. Chem. Phys. 81 (2003) 134–142.
[3] H. Mitsuyasu, K. Eguchi, H. Arai, Microscopic analysis of lanthanum strontium manganite/yttria-stabilized zirconia interface, Solid State Ionics 100 (1997) 11–15.
[4] A. Mitterdorfer, L.J. Gauckler, $La_2Zr_2O_7$ formation and oxygen reduction kinetics of the $La_{0.85}Sr_{0.15}Mn_yO_3$, O_2(g)|YSZ system, Solid State Ionics 111 (1998) 185–218.
[5] M. Chen, Y.-L. Liu, A. Hagen, P.V. Hendriksen, F.W. Poulsen, LSM–YSZ reactions in different atmospheres, Fuel Cells 9 (2009) 833–840.
[6] J.V. Spirig, J.L. Routbort, D. Singh, G. King, P.M. Woodward, P.K. Dutta, Joining of highly aluminum-doped lanthanum strontium manganese oxide with tetragonal zirconia by plastic deformation, Solid State Ionics 179 (2008) 550–557.
[7] K.E. Pappacena, D. Singh, E.V. Timofeeva, J.L. Routbort, Reaction joining of aluminum-doped lanthanum strontium manganese oxide to yttria-stabilized tetragonal zirconia for gas sensor applications, Int. J. Appl. Ceram. Technol. 9 (2012) 725–732.
[8] J. Holc, D. Kuščer, M. Hrovat, S. Bernik, D. Kolar, Electrical and microstructural characterization of $(La_{0.8}Sr_{0.2})(Fe_{1-x}Al_x)O_3$ and $(La_{0.8}Sr_{0.2})(Mn_{1-x}Al_x)O_3$ as possible SOFC cathode materials, Solid State Ionics 95 (1997) 259–268.
[9] S. Zhuiykov, Electrochemistry of Zirconia Gas Sensors, first ed., CRC Press, Florida, 2008.
[10] R. Ramamoorthy, S.A. Akbar, P.K. Dutta, Dependence of potentiometric oxygen sensing characteristics on the nature of electrodes, Sens. Actuators B 113 (2006) 162–168.

[11] Q. Hu, T. Jacobsen, K.V. Hansen, M. Mogensen, Lifetime of the internal reference oxygen sensor, Solid State Ionics 240 (2013) 34–40.
[12] H. Kaneko, T. Okamura, H. Taimatsu, Y. Matsuki, H. Nishida, Performance of a miniature zirconia oxygen sensor with a Pd-PdO internal reference, Sens. Actuators B 108 (2005) 331–334.
[13] E. van Setten, T.M. Gur, D.H.A. Blank, J.C. Bravman, M.R. Beasley, Miniature Nernstian oxygen sensor for deposition and growth environments, Rev. Sci. Instrum. 73 (2002) 156–161.
[14] S. Zhuiykov, 'In situ' diagnostics of solid electrolyte sensors measuring oxygen activity in melts by a developed impedance method, Meas. Sci. Technol. 17 (2006) 1570–1578.
[15] J.V. Spirig, R. Ramamoorthy, S.A. Akbar, J.L. Routbort, D. Singh, P.K. Dutta, High temperature zirconia oxygen sensor with sealed metal/metal oxide internal reference, Sens. Actuators B 124 (2007) 192–201.
[16] J. Prado-Gonjal, Á.M. Arévalo-López, E. Morán, Microwave-assisted synthesis: a fast and efficient route to produce $LaMO_3$ (M = Al, Cr, Mn, Fe, Co) perovskite materials, Mater. Res. Bull. 46 (2011) 222–230.
[17] M.S. Anwar, S. Kumar, F. Ahmed, G.W. Kim, B.H. Koo, Microwave assisted hydrothermal synthesis and magnetocaloric properties of $La_{0.67}Sr_{0.33}MnO_3$ manganite, J. Nanosci. Nanotechnol. 12 (2012) 5523–5526.
[18] J.C. Debnath, R. Zeng, A.M. Strydom, J.Q. Wang, S.X. Dou, Ideal Ericsson cycle magnetocaloric effect in $(La_{0.9}Gd_{0.1})_{0.67}Sr_{0.33}MnO_3$ single crystalline nanoparticles, J. Alloys Compd. 555 (2013) 33–38.
[19] X. Li, K.T. Jacob, G.M. Kale, La-doped $Ba_2In_2O_5$ electrolyte: Pechini synthesis, microstructure, electrical conductivity, and application for CO gas sensing, J. Electrochem. Soc. 157 (2010) J285–J292.
[20] G. Dercz, K. Prusik, L. Pajak, Structure investigations of commercial zirconia ceramic powder, J. Achiev. Mater. Manuf. Eng. 18 (2006) 259–262.
[21] R.E. Juárez, D.G. Lamas, G.E. Lascalea, N.E. Walsöe de Reca, Synthesis of nanocrystalline zirconia powders for TZP ceramics by nitrate-citrate combustion route, J. Eur. Ceram. Soc. 20 (2000) 133–138.
[22] F. Gutierrez-Mora, K.C. Goretta, N. Chen, J.L. Routbort, Joining advanced ceramics by plastic flow, Ceram. Int. 30 (2004) 1945–1948.
[23] F. Gutierrez-Mora, K.C. Goretta, S. Majumdar, J.L. Routbort, M. Grimdisch, A. Dominguez-Rodriguez, Influence of internal stresses in superplastic joining of zirconia toughened alumina, Acta Mater. 50 (2002) 3475–3486.
[24] N. Chen, F. Gutierrez-Mora, R.E. Koritala, K.C. Goretta, J.L. Routbort, J. Pan, Joining particulate and whisker ceramic composites by plastic flow, Compos. Struct. 57 (2002) 135–139.
[25] K.C. Goretta, F. Gutierrez-Mora, J.J. Picciolo, J.L. Routbort, Joining alumina/zirconia ceramics, Mater. Sci. Eng. A 341 (2003) 158–162.
[26] F. Gutierrez-Mora, J.L. Routbort, Electrical characterization of a joined electroceramic, $La_{0.85}Sr_{0.15}MnO_3$, J. Am. Chem. Soc. 85 (2002) 2370–2372.
[27] A. Dominguez-Rodriguez, F. Gutierrez-Mora, M. Jimenez-Melendo, J.L. Routbort, R. Chaim, Current understanding of superplastic deformation of Y-TZP and its application to joining, Mater. Sci. Eng. A 302 (2001) 154–161.
[28] M. Jiménez-Melendo, A. Domínguez-Rodríguez, A. Bravo-León, Superplastic flow of fine-grained yttria-stabilized zirconia polycrystals: constitutive equation and deformation mechanisms, J. Am. Ceram. Soc. 81 (1998) 2761–2776.
[29] K. Nomura, S. Tanase, Electrical conduction behavior in $(La_{0.9}Sr_{0.1})M^{III}O_{3-\delta}$ (M^{III} = Al, Ga, Sc, In, and Lu) perovskites, Solid State Ionics 98 (1997) 229–236.
[30] P.S. Anderson, F.M.B. Marques, D.C. Sinclair, A.R. West, Ionic and electronic conduction in $La_{0.95}Sr_{0.05}GaO_{3-\delta}$, $La_{0.95}Sr_{0.05}AlO_{3-\delta}$, and $Y_{0.95}Sr_{0.05}AlO_{3-\delta}$, Solid State Ionics 118 (1999) 229–239.
[31] M. Marinšek, Electrical conductivity of sintered LSM ceramics, Mater. Technol. 43 (2009) 79–84.

Biographies

Max R. Mullen is a doctoral student at The Ohio State University. His research interests involve high temperature sensors for gas phase species, the materials surrounding their design, and bonding processes and technology.

John V. Spirig received his PhD in chemistry from The Ohio State University. After a five-year career in pharmaceutical development at Bristol-Myers Squibb, John received an MBA from New York University and transitioned from science to strategy consulting. He is currently the director of a healthcare consultancy specializing in launch, growth, and post-LOE strategy development in the pharmaceutical industry.

Julia Hoy received her master's degrees in chemistry and education from the Ohio State University. She is currently a science teacher at Mechanicsburg High School in Mechanicsburg, Ohio.

Jules L. Routbort received his Ph.D. from Cornell University in Engineering Physics. He was a Senior Scientist at Argonne National Laboratory with expertise in the area of mechanical and transport properties of ceramic materials. Unfortunately, he passed away during the course of this work.

Dileep Singh currently serves as the Group Leader for Thermal-Mechanical Research at Argonne National Laboratory's Center for Transportation Research. He received his Ph.D. in Materials Science from the University of Utah. His research interests include materials and systems for thermal management, energy storage, and energy efficiency.

Prabir K. Dutta received his Ph.D. degree in chemistry from Princeton University. After four years of industrial research at Exxon Research and Engineering Company, he joined The Ohio State University, where currently he is professor of chemistry. His research interests are in the area of microporous materials, including their synthesis, structural analysis and as hosts for chemical and photochemical reactions.